LANGMUIR

pubs.acs.org/Langmuir Article

Measuring Local p K_a and pH Using Surface Enhanced Raman Spectroscopy of 4-Mercaptobenzoic Acid

Yu Yun Wang, Haotian Shi, Yichen Gong, Boxin Zhang, Bofan Zhao, Ruoxi Li, and Stephen B. Cronin*



Cite This: https://doi.org/10.1021/acs.langmuir.3c02073



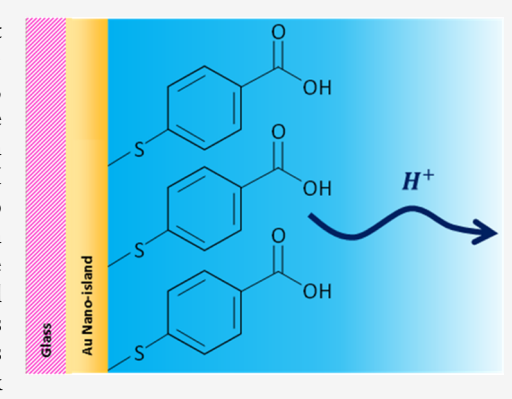
ACCESS I

III Metrics & More

Article Recommendations

Supporting Information

ABSTRACT: We report spectroscopic measurements of the local pH and p K_a at an electrode/electrolyte interface using surface enhanced Raman scattering (SERS) spectroscopy of 4-mercaptobenzoic acid (4-MBA). In acidic and basic solutions, the protonated and deprotonated carboxyl functional groups at the electrode surface exist in the solution as -COOH and $-\text{COO}^-$, which have different Raman active vibrational features at around 1697 and 1414 cm⁻¹, respectively. In pH neutral water, as the applied electrochemical potential is varied from negative to positive, the acidic form of the 4-MBA (*i.e.*, -COOH) decreases in Raman intensity and the basic form (*i.e.*, $-\text{COO}^-$) increases in Raman intensity. The change in local ion concentration is due to the application of electrochemical potentials and the accumulation of ions near the electrode surface. Under various applied potentials, the ratio of 1697 and 1587 cm⁻¹ (pH-independent) peak areas spans the range between 0.7 and 0, and the ratio of the 1414 and 1587 cm⁻¹ peak



areas ranges from 0 to 0.3. By fitting these data to a normalized sigmoid function, we obtain the percentage of surface protonation/deprotonation, which can be related to the pK_a and pH of the system. Thus, we can measure the local pK_a at the electrode surface using the surface enhanced Raman signal of the 4-MBA.

■ INTRODUCTION

Establishing the local pH/ion concentration near an electrode surface has been a longstanding problem in electrochemistry and photoelectrochemistry. Since pH is an inherently threedimensional quantity, there is no straightforward method on how to quantify this at an inherently two-dimensional interface. The local pH or ion concentration at the surface of an electrode can differ substantially from that of the bulk solution, which can affect the reaction energetics, field strengths, and kinetics of electrochemical processes. As such, these local ion concentrations and pH values at electrode surfaces play an important role in controlling the selectivity of electrochemical and photoelectrochemical reactions, like CO₂ reduction, which typically compete with the hydrogen evolution reaction (HER). Several attempts have been made to quantify the local pH and ion concentrations at electrode surfaces. However, most of these analyses have been inaccurate or invasive. Auinger et al. used a rotating platinum disc electrode to measure the near-surface ion distribution and effects of buffering in electrochemical reactions such as the HER and the hydrogen oxidation reaction. 1-3 These rotating electrode studies provide a basic understanding of surface pH but could not be directly applied to realistic scenarios in electrochemistry. Cathode surface concentrations have been calculated by Gupta et al. in the electrochemical reduction of CO₂ in KHCO₃ solutions. In their work, a pH variation of 4.25 was measured within 30 μm of the electrode surface. Surface pH measurements were also performed during

electrolysis using a rotating pH electrode, providing spatial resolution on the order of tens of microns. Leenheer and Atwater performed imaging of HER electrocatalyst surfaces using confocal fluorescence microscopy, using a pH indicator dye sensitive over the pH range from 5.3 to 7.5. 4-mercaptobenzoic acid (4-MBA) has been explored for intracellular and bulk pH sensing, due to its pH-sensitive Raman spectra; however, no studies have been performed at an electrochemical interface. 8-10

To provide SERS enhancement, the molecule can be bounded to various plasmonic nanostructures, including silver nanoparticles, gold nanoshells, and nanoaggregated hollow gold nanospheres (HGNSs). In the work presented here, we demonstrate a novel method to measure local pH using surface enhanced Raman spectroscopy of 4-MBA on gold nanoislands. In situ spectroscopy of surface reporter molecules has emerged as a hot topic in recent years, with many of the top research groups publishing papers in high impact journals. However, a vast majority of these papers involve measurement of the local electric field via vibrational Stark-shift spectroscopy, for

Received: August 2, 2023 Revised: October 11, 2023 Accepted: October 17, 2023



example, using 4-mercaptobenzonitrile (MBN), rather than local ion concentrations. $^{13-16}$

In the work presented here, we have developed a framework for determining pK_a , which is a well-defined quantity at the 2D electrode surface by using surface-bound molecules that report pK_a within 1 nm of the surface. This is a facile technique that can be attained with commercially available molecules and a turn-key Raman spectrometer, requiring no special skills or expertise. This stands in contrast to other techniques such as sum frequency generation spectroscopy 14,17 and surface enhanced IR absorption spectroscopy (SEIRAS), which require specialized equipment and advanced technical skills.

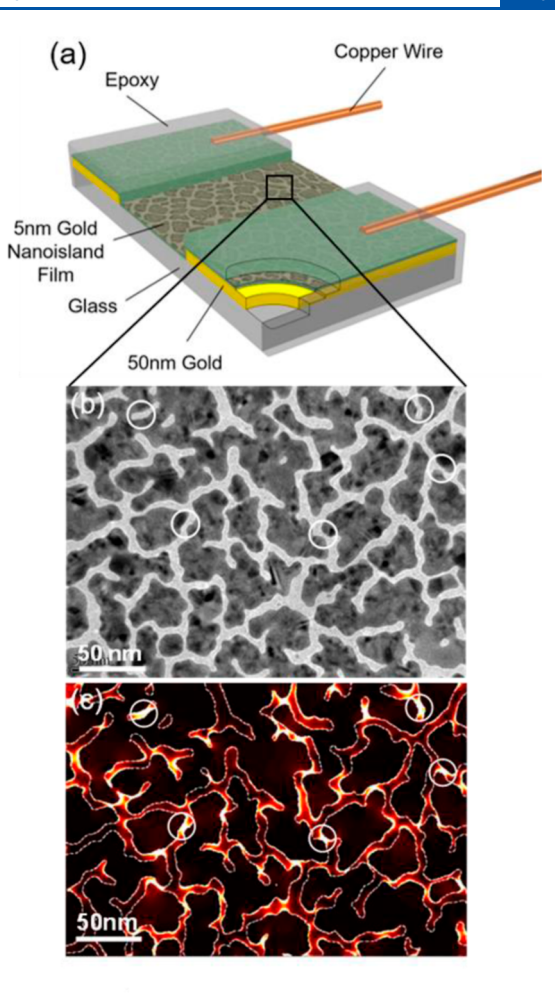
■ EXPERIMENTAL DETAILS

The electrodes used in our work are fabricated using the following procedure. Glass slides (VWR Cat. no. 48300-048) are cleaned with 10% hydrochloric acid in DI water, followed by baking on a hot plate at 120 °C for 10 min.²⁰ Prior to depositing the gold nanoislands, two gold electrodes (50 nm thick) are deposited on the glass substrate by electron-beam evaporation using a shadow mask (gold pellets: Au, 99.999%, 1/8" Dia. x 1/8" Length, Part no. EVMAUXX50G, Kurt J. Lesker Company). A 5 nm (nominal thickness) Au film is then deposited on the sample using electron-beam evaporation, which results in the formation of gold nanoislands that are strongly plasmonic.²¹ The gold nanoisland electrode (1 cm \times 1 cm) typically has an in-plane resistance of 50 Ω , as illustrated in Figure 1. A thin layer of 4-mercaptobenzonic acid (4-MBA) molecules (Sigma-Aldrich #706329) is self-assembled on the surface of the gold nanoislands by soaking the sample in a 0.03 mol/L solution of 4-MBA in ethanol for 24 h, 14,17 resulting in the structure illustrated in Figure 1a-c. After 4-MBA deposition, the sample was rinsed in DI water twice and immersed in the DI water for the in situ electrochemical measurements. Copper wires are attached to the gold electrodes and are used as the working electrode in a three-terminal potentiostat, as illustrated in Figure 1a. The contact area between the copper wires and gold electrodes (coated with silver paint) are encapsulated in epoxy in order to insulate them from the electrolyte.

Raman spectra of the surface-bound 4-MBA were taken with 633 nm wavelength excitation, which is resonant with the gap plasmon modes of the Au nanoislands. 22,23 633 and 785 nm wavelength excitation have been predominantly used in Raman measurements of 4-MBA molecules. 24 Electrochemical potentials were applied in pure DI water using a water immersion lens, as illustrated in Figure 1d. In order to protect the lens from the solution, it was covered with a 13 μ m-thick Teflon sheet (American Durafilm, Inc.). A three terminal potentiostat (Gamry, Inc.) was used to apply various electrochemical potentials to the working electrode with respect to the reference electrode. A silver/silver chloride reference electrode and glassy carbon electrode (SPI, Inc.) were used as the reference and counter electrodes, respectively.

■ RESULTS AND DISCUSSION

Figure 2b shows the Raman spectra of surface bound 4-MBA in acidic and basic solutions. Here, we observe two dominant peaks around 1590 and 1080 cm⁻¹, which can be assigned to the ν_{8a} and ν_{12} aromatic ring vibrations, respectively.⁸ In pH = 2 solution (0.005 M H₂SO₄), we observe a vibrational mode around 1697 cm⁻¹ corresponding to the protonated carboxyl group (COOH). In pH = 12 solution (0.01 M KOH), we observe a vibrational mode at 1414 cm⁻¹ corresponding to the deprotonated carboxyl group (COO⁻). Previously, Kneipp *et al.*²⁵ measured the relative intensities of the COO⁻ and COOH peaks as a function of bulk solution pH, however, without an applied electrochemical potential. Figure 2c shows the normalized Raman intensities of the COO⁻ and COOH peaks observed in pH neutral DI water plotted as a function of



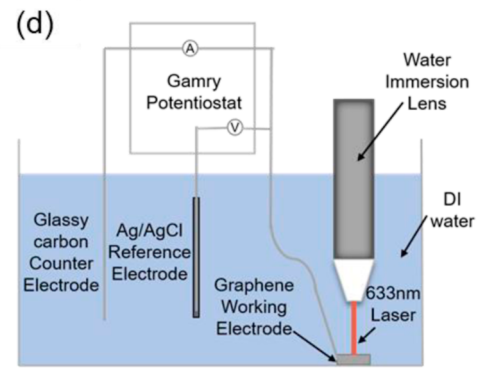


Figure 1. (a) Illustration of the SERS-active Au nanoisland electrode. (b) Transmission electron microscope image and (c) electric field intensity distribution of the gold nanoisland film calculated by the finite difference time domain method. (d) Schematic diagram of the three-terminal electrochemical cell using a water immersion lens to collect *in situ* Raman spectra.

the applied potential. Under oxidative conditions, *i.e.* + 0.4 V vs Ag/AgCl, we only observe the deprotonated peak COO⁻, indicating that the local pH is basic. Similarly, under reducing conditions, *i.e.* -0.8 V vs Ag/AgCl, we only observe the protonated peak COOH, indicating that the local pH is acidic.

Since pH is an inherently three-dimensional quantity, it is difficult to assign a "local pH" value to each applied potential at the electrode/electrolyte interface, which is inherently two-dimensional. Instead, we can determine the percentage of surface protonation and deprotonation at each applied

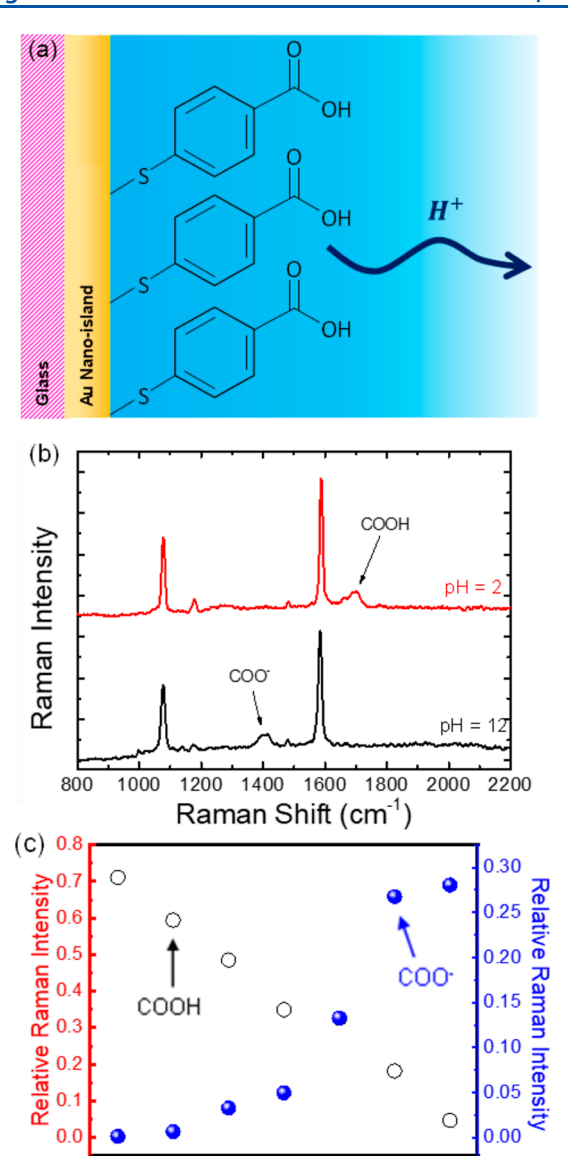


Figure 2. (a) Schematic diagram of 4-mercaptobenzoic acid (4-MBA) grafted gold nanoisland in aqueous solution. (b) Raman spectra of 4-MBA grafted gold nanoisland in 0.01 M KOH solution (pH = 12) and in 0.005 M H2SO4 solution (pH = 2). (c) Relative Raman intensities of the -COOH and $-COO^-$ characteristic peaks with respect to the pH-insensitive peak at 1587 cm⁻¹ plotted as a function of the electrochemical potential in DI water.

Potential vs. Ag/AgCI (V)

-0.6

-0.4 -0.2

potential, as plotted in Figure 3. This was achieved by first normalizing the intensities of the COO⁻ and COOH peaks with respect to the pH-insensitive Raman peak of 1587 cm⁻¹ associated with the aromatic ring vibrational modes. These relative Raman intensities are then fit to a potential-dependent, normalized sigmoid function spanning from 0 to 100% surface protonation/deprotonation. Based on the mass action kinetic model, the equilibrium constant K_a , i.e., the ratio of products to reactants, can be related to the ratio of the rate constant of deprotonation k_d to protonation k_a , as $K_a = k_d/k_a = [COO^-][H^+]/[COOH]$. The fraction of the surface reporter molecules that are protonated or deprotonated, i.e., $[COOH]/([COO^-] + [COOH])$) or $[COO^-]/([COO^-] + [COOH])$, can be related to $[H^+]/(K_a + [H^+])$ or $K_a/(K_a + [H^+])$,

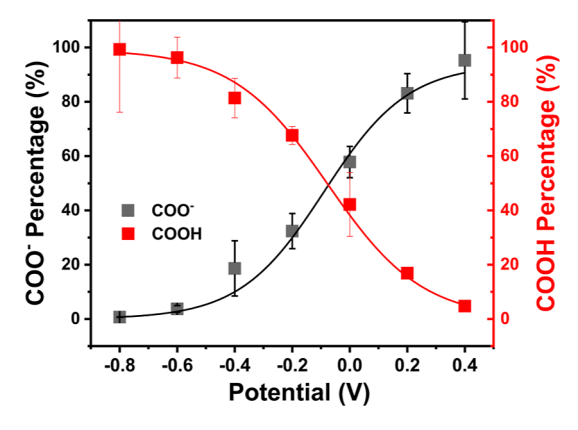


Figure 3. Normalized sigmoid function of the -COOH and -COO⁻ percentage spanning from 0 to 100% surface protonation/ deprotonation plotted as a function the electrochemical potential in DI water.

respectively. Since the Raman intensity is proportional to the density of molecules, the fractions mentioned above are proportional to the Raman intensities of the protonated or deprotonated species I_{1697} or I_{1414} divided by the Raman intensity of the parent species I_{1587} . Thus, the ratio of the protonated Raman intensity I_{1697} or the deprotonated Raman intensity I_{1414} to the Raman intensity of the parent molecules I_{1587} can be expressed as

$$\frac{I_{1697}}{I_{1587}} = \frac{A_1}{1 + \exp^{-\ln 10^* [pK_a - pH]}}$$
(1)

$$\frac{I_{1414}}{I_{1587}} = \frac{A_2}{1 + \exp^{-\ln 10^* [pH - pK_a]}}$$
 (2)

where A_1 and A_2 are the coefficients relating ratio of the concentration to the Raman-intensity of the protonated/deprotonated groups to the parent molecules. Since the equilibrium constant $K_{\rm a}$ changes with the applied electrochemical potentials, the Raman intensity-to-concentration ratio of the protonated/deprotonated groups to the parent molecules can be expressed as

$$S(x) = \frac{a}{1 + \exp^{-k(x - x_c)}}$$
 (3)

where the coefficient a is the fitted ratio of the Raman intensity-to-concentration coefficients of the protonated/ deprotonated groups to the pH-insensitive aromatic parents, k is the shape parameter, and x_c is the applied condition when the protonated and deprotonated species both reach 50%. To further obtain the surface density of the protonated/ deprotonated species, the normalized Raman intensities shown in Figure 2c are renormalized by the fitted coefficient, a, from eq 3. Since the amount of the 4-MBA reporters attached on the electrode remains the same for a lossless system, the sum of the surface density of the COO and COOH at each applied electrochemical potential should be the same as the surface density of the parent 4-MBA molecules. Therefore, the sigmoid normalized COO⁻ and COOH Raman intensities can be converted to the percentages shown in Figure 3.

To further obtain the surface equilibrium constant of the 4-MBA on gold nanoislands, we can express the equilibrium reaction as nanogold-S-aromatic ring-COOH_(s) \rightleftharpoons nanogold-S-

aromatic ring- $COO^-_{(s)} + H^+_{(aq)}$ with an associated surface equilibrium constant K_a given by

$$pK_{a,surface} = -\log\left(\frac{[COO^{-}][H^{+} \text{ per volume}]}{[COOH]}\right) \text{ or } pK_{a,surface}$$
$$= -\log\left(\frac{COO^{-}(\%)}{COOH(\%)}\right) + pH$$
(4)

Equation 4 enables us to relate the observed Raman spectra to the p K_a and pH of the system. Figure 4 shows p $K_{a,surface}$ plotted

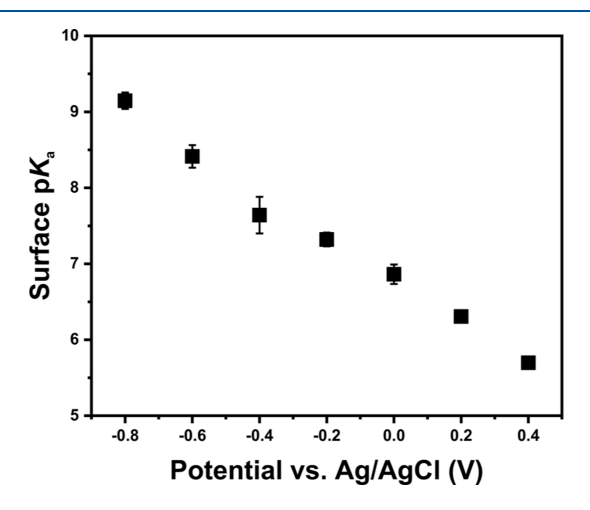


Figure 4. Electrode/electrolyte interface pKa, surface plotted as a function of the applied potential in DI water.

as a function of the applied potential, assuming a bulk pH value of 7. Under these conditions, the value of $pK_{a,surface}$ ranges from 6 to 9 in our system. It should be noted that thiols may undergo reductive desorption at negative applied potentials in an aqueous solution. However, the pH-insensitive Raman peak at $1587~\mathrm{cm}^{-1}$ associated with the aromatic ring vibration mode of 4-MBA remains nearly constant in Raman intensity when subjected to negative electrochemical potentials, as shown in Figure S2. Since SERS is a surface-sensitive technique, no change in the Raman intensity implies that there is no desorption taking place over the applied potential range. It has been previously established that the reductive desorption of 4-MBA from gold electrodes occurs at a potential of -0.9 to -1.0 V vs SSE.²⁶ To induce reductive desorption of 4-MBA on the gold nanoislands, an electrochemical potential lower than −0.9 V vs SSE is necessary. Consequently, the 4-MBA monolayer remains unaffected by any reductive desorption at negative potentials, even down to −0.8 V vs Ag/AgCl.

CONCLUSIONS

In conclusion, spectroscopic measurements of the local pH at an electrode/electrolyte interface are reported using surface enhanced Raman spectroscopy of 4-mercaptobenzoic acid. In acidic and basic environments, the carboxyl functional group exists in the solution as the protonated and deprotonated forms of -COOH and -COO⁻, which have different characteristic Raman peaks at 1697 and 1414 cm⁻¹, respectively. When various electrochemical potentials are applied in DI water, the relative intensities of these two peaks changes. Given the abundance of DI water relative to the released H⁺ from 4-MBA functionalized gold nanoislands, the pH of the system is fixed at 7. This fixed pH of DI water serves

as a reference point for determining the pK_a value in our system, providing surface pK_a sensitivity over the range of 6–9. This approach provides a measure of the local pK_a within 1 nm of the electrode surface using the surface enhanced Raman signal of the 4-MBA.

ASSOCIATED CONTENT

Supporting Information

The Supporting Information is available free of charge at https://pubs.acs.org/doi/10.1021/acs.langmuir.3c02073.

Top-view diagram and SEM image of plasmonic gold nanoisland electrode; pH-insensitive peak at 1587 cm $^{-1}$ of 4-MBA when subjected to negative electrochemical potentials; relation of p $K_{\rm a,surface}$ to the applied potentials in DI water (PDF)

AUTHOR INFORMATION

Corresponding Author

Stephen B. Cronin — Ming Hsieh Department of Electrical Engineering, University of Southern California, Los Angeles, California 90089, United States; Department of Chemistry, University of Southern California, Los Angeles, California 90089, United States; orcid.org/0000-0001-9153-7687; Email: scronin@usc.edu

Authors

Yu Yun Wang — Ming Hsieh Department of Electrical Engineering, University of Southern California, Los Angeles, California 90089, United States; orcid.org/0000-0003-0620-5069

Haotian Shi – Department of Chemistry, University of Southern California, Los Angeles, California 90089, United States

Yichen Gong — Department of Chemical Engineering, University of Southern California, Los Angeles, California 90089, United States

Boxin Zhang — Department of Materials Science, University of Southern California, Los Angeles, California 90089, United States

Bofan Zhao - Ming Hsieh Department of Electrical Engineering, University of Southern California, Los Angeles, California 90089, United States; ○ orcid.org/0000-0003-0478-6330

Ruoxi Li — Department of Materials Science, University of Southern California, Los Angeles, California 90089, United States; orcid.org/0000-0002-6432-6072

Complete contact information is available at: https://pubs.acs.org/10.1021/acs.langmuir.3c02073

Notes

The authors declare no competing financial interest.

ACKNOWLEDGMENTS

This research was supported by the U.S. Department of Energy, Office of Basic Energy Sciences award no. DESC0019322 (Y.Y.W.), the Army Research Office (ARO) award no. W911NF-22-1-0284 (B.Z.), National Science Foundation (NSF) award nos. CHE-2106480 (H.S.) and CBET-2012845 (R.L.), and Air Force Office of Scientific Research (AFOSR) grant no. FA9550-19-1-0115 (B.Z.).

REFERENCES

- (1) Auinger, M.; Katsounaros, I.; Meier, J. C.; Klemm, S. O.; Biedermann, P. U.; Topalov, A. A.; Rohwerder, M.; Mayrhofer, K. J. J. Near-surface ion distribution and buffer effects during electrochemical reactions. *Phys. Chem. Chem. Phys.* **2011**, *13* (36), 16384–16394.
- (2) Katsounaros, I.; Meier, J. C.; Klemm, S. O.; Topalov, A. A.; Biedermann, P. U.; Auinger, M.; Mayrhofer, K. J. J. The effective surface pH during reactions at the solid-liquid interface. *Electrochem. Commun.* **2011**, *13* (6), 634–637.
- (3) Rossrucker, L.; Samaniego, A.; Grote, J. P.; Mingers, A. M.; Laska, C. A.; Birbilis, N.; Frankel, G. S.; Mayrhofer, K. J. J. The pH Dependence of Magnesium Dissolution and Hydrogen Evolution during Anodic Polarization. *J. Electrochem. Soc.* **2015**, *162* (7), C333–C339.
- (4) Gupta, N.; Gattrell, M.; MacDougall, B. Calculation for the cathode surface concentrations in the electrochemical reduction of CO2 in KHCO3 solutions. *J. Appl. Electrochem.* **2006**, 36 (2), 161–172.
- (5) Deligianni, H.; Romankiw, L. T. In situ surface pH measurement during electrolysis using a rotating pH electrode. *IBM J. Res. Dev.* **1993**, *37* (2), 85–95.
- (6) Romankiw, L. T. Technique for measuring pH at electrodes during electrolysis. J. Electrochem. Soc. 1970, 117 (3), C118.
- (7) Leenheer, A. J.; Atwater, H. A. Imaging Water-Splitting Electrocatalysts with pH-Sensing Confocal Fluorescence Microscopy. *J. Electrochem. Soc.* **2012**, *159* (9), H752–H757.
- (8) Michota, A.; Bukowska, J. Surface-enhanced Raman scattering (SERS) of 4-mercaptobenzoic acid on silver and gold substrates. *J. Raman Spectrosc.* **2003**, 34 (1), 21–25.
- (9) Talley, C. E.; Jusinski, L.; Hollars, C. W.; Lane, S. M.; Huser, T. Intracellular pH Sensors Based on Surface-Enhanced Raman Scattering. *Anal. Chem.* **2004**, *76* (23), 7064–7068.
- (10) Lee, S. B.; Kim, K.; Kim, M. S. Surface-enhanced Raman scattering of o-mercaptobenzoic acid in silver sol. *J. Raman Spectrosc.* **1991**, 22 (12), 811–817.
- (11) Bishnoi, S. W.; Rozell, C. J.; Levin, C. S.; Gheith, M. K.; Johnson, B. R.; Johnson, D. H.; Halas, N. J. All-Optical Nanoscale pH Meter. *Nano Lett.* **2006**, *6* (8), 1687–1692.
- (12) Schwartzberg, A. M.; Oshiro, T. Y.; Zhang, J. Z.; Huser, T.; Talley, C. E. Improving Nanoprobes Using Surface-Enhanced Raman Scattering from 30-nm Hollow Gold Particles. *Anal. Chem.* **2006**, *78* (13), 4732–4736.
- (13) Guo, W.; Liu, B.; He, Y.; You, E.; Zhang, Y.; Huang, S.; Wang, J.; Wang, Z. Plasmonic Gold Nanohole Arrays for Surface-Enhanced Sum Frequency Generation Detection. *Nanomaterials (Basel)* **2020**, 10 (12), 2557.
- (14) Patrow, J. G.; Sorenson, S. A.; Dawlaty, J. M. Direct Spectroscopic Measurement of Interfacial Electric Fields near an Electrode under Polarizing or Current-Carrying Conditions. *J. Phys. Chem. C* **2017**, *121* (21), 11585–11592.
- (15) Schkolnik, G.; Utesch, T.; Zhao, J.; Jiang, S.; Thompson, M. K.; Mroginski, M. A.; Hildebrandt, P.; Franzen, S. Catalytic efficiency of dehaloperoxidase A is controlled by electrostatics-application of the vibrational Stark effect to understand enzyme kinetics. *Biochem. Biophys. Res. Commun.* 2013, 430 (3), 1011–1015.
- (16) Suo, S.; Sheehan, C.; Zhao, F.; Xiao, L.; Xu, Z.; Meng, J.; Mallouk, T. E.; Lian, T. Direct Vibrational Stark Shift Probe of Quasi-Fermi Level Alignment in Metal Nanoparticle Catalyst-Based Metal-Insulator-Semiconductor Junction Photoelectrodes. *J. Am. Chem. Soc.* 2023, 145 (26), 14260–14266.
- (17) Humbert, C.; Busson, B.; Six, C.; Gayral, A.; Gruselle, M.; Villain, F.; Tadjeddine, A. Sum-frequency generation as a vibrational and electronic probe of the electrochemical interface and thin films. *J. Electroanal. Chem.* **2008**, *621* (2), 314–321.
- (18) Rudnev, A. V.; Zhumaev, U.; Utsunomiya, T.; Fan, C. J.; Yokota, Y.; Fukui, K.; Wandlowski, T. Ferrocene-terminated alkanethiol self-assembled monolayers: An electrochemical and in situ surface-enhanced infra-red absorption spectroscopy study. *Electrochim. Acta* **2013**, *107*, 33–44.

- (19) Tu, K. Y.; Morhart, T. A.; Read, S. T.; Rosendahl, S. M.; Burgess, I. J. Probing Heterogeneity in Attenuated Total Reflection Surface-Enhanced Infrared Absorption Spectroscopy (ATR-SEIRAS) Response with Synchrotron Infrared Microspectroscopy. *Appl. Spectrosc.* **2021**, 75 (9), 1198–1206.
- (20) Chen, C. C.; Chang, C. C.; Li, Z.; Levi, A. F. J.; Cronin, S. B. Gate tunable graphene-silicon Ohmic/Schottky contacts. *Appl. Phys. Lett.* **2012**, *101* (22), 223113.
- (21) Shi, H.; Poudel, N.; Hou, B.; Shen, L.; Chen, J.; Benderskii, A. V.; Cronin, S. B. Sensing local pH and ion concentration at graphene electrode surfaces using in situ Raman spectroscopy. *Nanoscale* **2018**, *10* (5), 2398–2403.
- (22) Liu, Z.; Hou, W.; Pavaskar, P.; Aykol, M.; Cronin, S. B. Plasmon Resonant Enhancement of Photocatalytic Water Splitting Under Visible Illumination. *Nano Lett.* **2011**, *11* (3), 1111–1116.
- (23) Pavaskar, P.; Hsu, I. K.; Theiss, J.; Hsuan Hung, W.; Cronin, S. B. A microscopic study of strongly plasmonic Au and Ag island thin films. *J. Appl. Phys.* **2013**, *113* (3), 034302.
- (24) Guo, L.; Mao, Z.; Jin, S.; Zhu, L.; Zhao, J.; Zhao, B.; Jung, Y. M. A SERS Study of Charge Transfer Process in Au Nanorod-MBA@ Cu2O Assemblies: Effect of Length to Diameter Ratio of Au Nanorods. *Nanomaterials* **2021**, *11* (4), 867.
- (25) Kneipp, J.; Kneipp, H.; Wittig, B.; Kneipp, K. One- and Two-Photon Excited Optical pH Probing for Cells Using Surface-Enhanced Raman and Hyper-Raman Nanosensors. *Nano Lett.* **2007**, 7 (9), 2819—2823.
- (26) Zangmeister, C. D.; Bertocci, U.; Beauchamp, C. R.; Stafford, G. R. In situ stress measurements during the electrochemical adsorption/desorption of self-assembled monolayers. *Electrochim. Acta* **2008**, *53* (23), *6778*–*6786*.